

# A Sky Image Analysis System for Sub-minute PV Prediction

Rodrigo Verschae\*, Li Li\*, Shohei Nobuhara\* and Takekazu Kato\*†

\*Graduate School of Informatics, Kyoto University, Kyoto, 606-8501, Japan

Email: {rodrigo,li,nob}@vision.kuee.kyoto-u.ac.jp

†Shizouka Institute of Science and Technology, Japan

Email: kato.takekazu@sist.ac.jp

**Abstract**—Advanced energy management systems are increasingly gaining importance. These systems will allow the further introduction of Photovoltaic (PV) power generation, but for them to be really effective, sub-minute (1-60 sec.) PV generation prediction is required. In this context we propose a sub-minute PV prediction system based on the analysis of sky images. This is done by analyzing cloud movement, and thus the system does not rely on i) historical PV data, ii) dynamic model of the local weather, nor iii) location dependent information. The proposed system works as follows: from multiple image exposures, high dynamic range images are obtained (one per second), cloud movement is estimated, sky images are predicted, and finally PV generation is estimated using the predicted sky images. The proposed system achieves low error under various weather conditions.

**Index Terms**—photovoltaic, prediction, sky image, sub-minute, high dynamic range, cloud movement.

## I. INTRODUCTION

In recent years, systems that greatly increase the energy management ability of each demand have been proposed. These systems enable the management of generation and consumption, e.g. allowing each end-point of the system to set power consumption targets, to follow fluctuating power sources, and to coordinate consumption and generation with other users (see e.g. [1] [2] [3]).

Another trend has been the rapid introduction of uncontrollable renewables (including PV) due to *i*) the lower cost of renewables and batteries, and *ii*) government policies encouraging their installation (e.g. the Fit-In Tariff (FIT) scheme). As a consequence, more consumers have installed their own generation, storage and energy management systems.

However, restrictions to the further installation of uncontrollable renewables due to the limited controllable generation capacity has been observed in some regions (e.g. in Kyushu, Japan). Moreover, the time-limit of FIT programs [4], may not allow users to continue injecting energy in to the grid, e.g. the FIT program for residential users in Japan lasts 10 years, and it is not clear what these users will do after the FIT program finishes.

To increase the introduction of PV, advanced energy management system are key, and such systems would greatly benefit by having a local sub-minute PV prediction. Thus, we address the problem of such sub-minute prediction PV.

The power generation of a PV system depends mainly on a single environmental factor: the relative position of the sun, the clouds, and the PV station. Thus, by analyzing the movement and position of the clouds with respect to

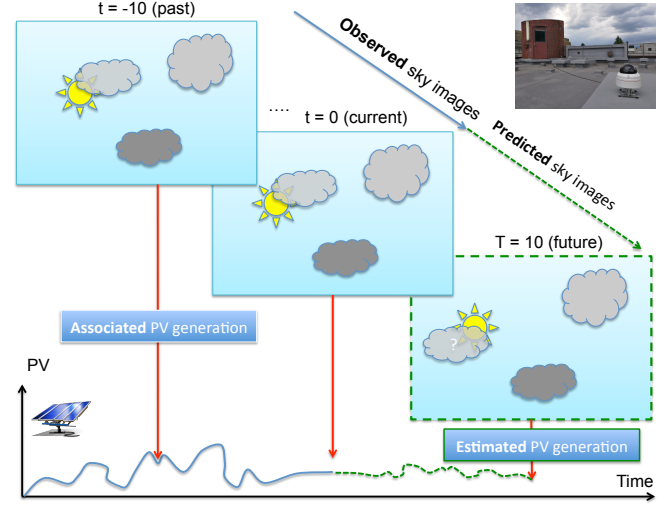


Fig. 1. Proposed Approach. To predict the PV generation, first future sky images are predicted, and later the PV power associated to the predicted sky image is estimated. Sky image prediction is done by analyzing cloud movement, thus his system does not require a historical data, nor dynamical model (of PV generation) nor geo-location information.

TABLE I  
OVERVIEW OF APPROACHES FOR PV PREDICTION [5][6].

Approach (Sensor)	Time Horizon	Resolution	RMSE
Weather model [7]	Hour-ahead	1 hour	20-60%
Satellite imaging [8]	Hour-ahead	1 minute	20%
Dynamic PV model [9], [10]	Intra-hour	15 minute	20%
Sky image (cloud mov.)	Intra-minute	1 second	(proposed)

the PV cell and the sun, it should possible to predict the PV generation at any location. In this line, we address the challenge of sub-minute PV prediction (time horizon of 1 - 60 sec.). In particular we investigate how to predict PV power generation using a camera facing up to the sky (see Fig. 1).

## II. RELATED WORK

Various approaches have been proposed to predict PV generation [5][6]. These are designed to work at various time scales, time resolutions, and spatial resolutions, with most methods performing a day-ahead prediction for every 30-minute. Most methods can be grouped in 3 categories (see Table 1): weather-based models, satellite imaging systems, and dynamical models (learned from historical PV data).

Numerical weather based models have low time & spatial resolution and are based on physical models. Satellite image methods directly use cloud structure, thus they do not rely on historical data or dynamical models, achieving a higher accuracy and working at smaller time scales (intra-hour PV prediction), but they have low spatial resolution. Satellite imaging has been used for intra-hour PV prediction based on the estimation of cloud structure and motion.

An alternative is to use PV measurements together with models learned from historical data (e.g. dynamical models auto-regressive (AR) models) [10][9]. In general these methods provide intra-hour (a 5 minute-ahead) PV prediction, but they are trained for each location using dynamical models learned using historical data. Given that measuring PV generation at a single location may not be enough, the use of distributed PV measurements has been recently proposed [8] [9]. Distributed PV measurements improve the PV prediction when compared to PV measurements at a single location, achieving intra-hour prediction, however these methods also require a location-specific model learned from historical data.

### III. SUB-MINUTE SKY IMAGE AND PV PREDICTION

To predict PV generation we propose to analyze and predict cloud movement from sky images and to estimate PV generation from these predicted images. An advantage of this approach is that it does not require historical data, dynamical model, nor geo-location. While the analysis of static sky images has been proposed [11], to the best of our knowledge, cloud movement for sub-minute PV prediction has not. The proposed system consists of four main parts:

- PV generation measurement,
- High Dynamic Range (HDR) sky image capture,
- Sky image analysis and prediction, and
- Image based PV power estimation.

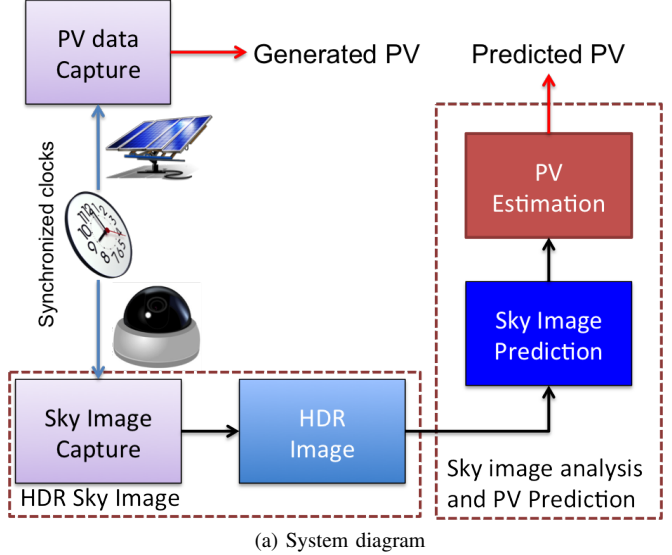
#### A. PV Generation System and Measurement

PV generation data is captured at 1-second resolution at a PV station. The PV cells are parallel to the ground and the station has generation capacity of 2500W. The generated power is sensed using a current transformer (CT) sensor and each sample is time-stamped with a NTP synchronized clock. The station is located 100mt from the image capture system.

#### B. Sky Image Capture System

*1) Capture System and High Dynamic Range Images:* The system captures multiple image exposures at a high speed (8 fps) that are combined to obtain the HDR image. The capture program is implemented in C++ and uses multi-thread programming to improve throughput and reduce I/O blocking. The images are cropped in camera (1280x1280 pixels) and captured using a bracketing mode that allows to iterate over 4 shutter speeds. Every half second 4 images are captured (with exposure times in  $\{1, 8, 16, 24\} \times 11ms$ , see Fig. 3).

In order to reduce cloud movement within a bracket, out of the eight frames captured every second, the first 4 frames are kept. These 4 frames are stored in TIFF format and then



(a) System diagram



(b) Camera system

Fig. 2. System diagram and camera system. The system consists basically of three main parts: PV data capture, Sky image capture and HDR image formation, and Sky image analysis (image prediction and pv estimation). The camera capture system consists of a CMOS Camera, a Fish-eye lens, and a housing to protect the camera (not shown in the image).

encoded as MP4 videos. These videos are later decoded and the exposures and combined to obtain the HDR image [12].

The system's hardware consists of:

- a CM3-U3-31S4C Chameleon3 PointGrey Camera (Sony IMX265, 1/1.8", Color, 2048x1536 (3.2MP), USB3),
- a Spacecom TV1634M, F1.4, 180 Fish-eye lens, and
- an Intel i7, 8 cores, 4 GHz, 32GB RAM PC (Ubuntu).

*2) Lens calibration:* We use a calibrated model of the camera-lens system that gives us the direction of each light ray being collected by each pixel. The lens is modeled using a 4th degree polynomial [13]:

$$f(\rho) = a_0 + a_1\rho + a_2\rho^2 + a_3\rho^3 + a_4\rho^4, \quad (1)$$

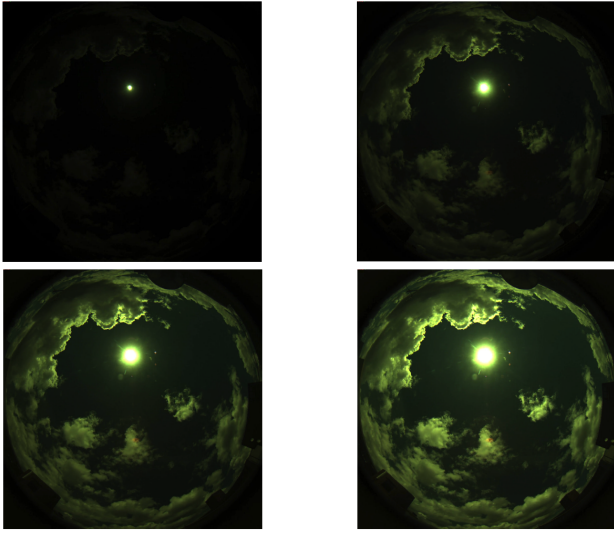


Fig. 3. Multiple exposures ( $\in 11 \times \{1, 8, 16, 24\}$ msec) are captured to generate a HDR image. Images as obtained from the camera. No color correction was applied, thus the greenish look (the sensor's efficiency varies across color channels, with the green channel having the highest quantum efficiency).

with  $\rho$  the distance from the center of the image ( $\rho = \sqrt{u^2 + v^2}$ ),  $(u, v)$  the coordinates in the sensor plane (in pixels). In this model,  $f(\rho)$  gives us the coordinate of the 3D point  $[u, v, f(\rho)]$  associated to sensor pixel  $(u, v)$ . Then, given the distance  $\rho$  of a pixel from the image center, we estimate the corresponding light direction  $\theta$  from:

$$\tan \theta = \rho / f(\rho). \quad (2)$$

This model is calibrated following [13] using a checkboard of known geometry. Fig. (4) presents calibration results.

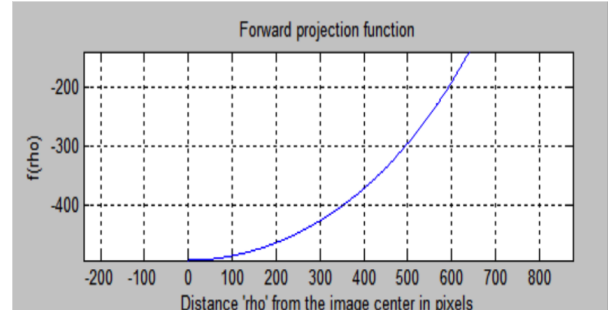
### C. Sky Image Analysis and Prediction

1) *Light projection model*: We consider a light projection model that maps the light to a plane in the sky (see Fig. 5a) because sub-minute cloud movement can be approximated as linear in this plane (in the original sensor plane, the cloud movement is not linear due to the fish-eye lens). The sun can be assumed to be static (within one minute). Fig. 5 presents an example of this mapping.

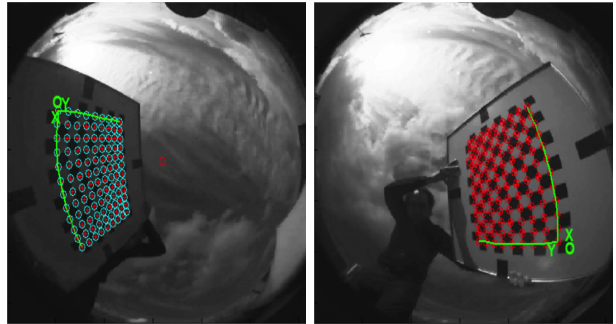
2) *Movement Analysis*: We use optical flow [14] to calculate the movement of each pixel, and we then use linear prediction using the calculate model. This is done in the sky plane projection, where the cloud movement can be assumed to be linear. Empty pixels can be observed (two pixels may move to the same location), and we obtain such empty pixels by interpolating neighbor values. The predicted image is projected back to the original image plane for the later PV Estimation.

### D. PV Estimation

To estimate PV generation from a sky image we need to consider the fish-eye lens light projection (in the sensor) and



(a) Mapping function  $f(\rho)$



(b) Checkboard and projected lines.

Fig. 4. Lens calibration. The calibrated model closely matches the checkboard patterns (projected lines (green) in (b)).

the cosine law (of the PV cell). Also we need to take into account camera sensor response, and in particular we need to consider that some pixels of the image saturate<sup>1</sup>. Pixel saturation is an important problem, specially during sunny days, as can be observed in Fig. 6. The PV estimation takes into account:

1) *Light incidence angle*: We integrate the light energy according to the unit projection sphere (Fig. 5a) using the calibrated lens model. For clarity, we use color channel  $c$ . Each pixel value  $I_c(u, v)$  is weighted considering the light ray direction for the pixel and the PV cell:

$$PV_w = \alpha_c \sum_{(u,v)} I_c(u, v) w(u, v), \quad (3)$$

where  $w(u, v) = w_a(u, v)w_b(u, v)$ . Here  $w_b(u, v)$  represents the weight of the spherical sector sampled by pixel  $(u, v)$  (for our fish-eye lens  $w_b(u, v)$  is constant), and  $w_a(u, v) = \cos \theta$  is the weight associated the angle of incidence in the PV cell. If we define  $\rho = \sqrt{u^2 + v^2}$ , the value of  $\theta$  is estimated from:

$$\tan(\theta) = \rho / f(\rho). \quad (4)$$

2) *Spectral response*: The PV cell spectral response and image sensor color channel have a specific spectral response.

<sup>1</sup>Note that while the HDR image helps reducing saturation the dynamic range of the light is too large to be handle by a standard camera.

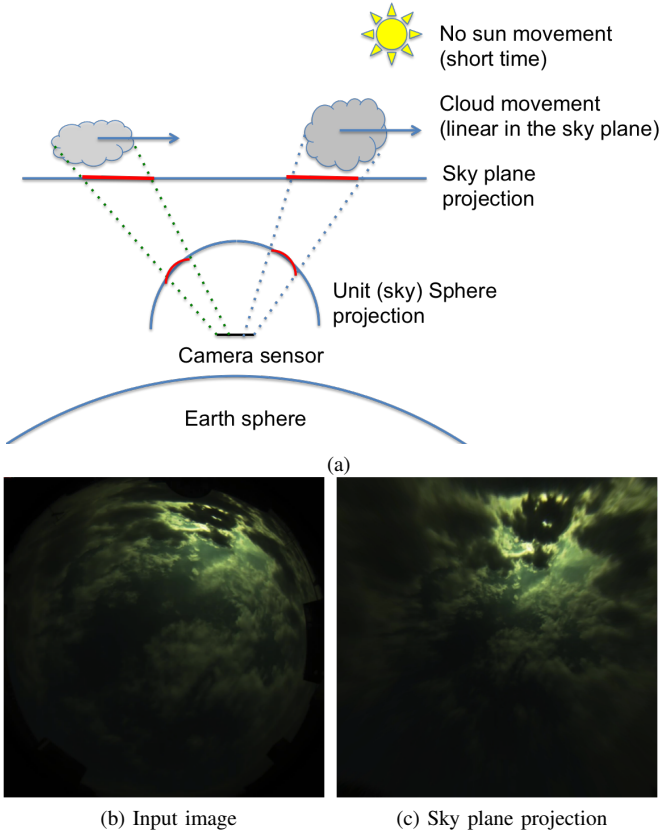


Fig. 5. (a) Light projection model: sensor, sphere and sky plane projections. The cloud movement is linear in the sky plane projection, thus it is used for cloud movement prediction. The unit sphere projection is used for PV estimation. (b) Original image (camera sensor) and (c) its sky plane projection.

To take them into account, the intensity of each color channel  $c \in \mathbb{C} = \{R, G, B\}$  is included in the PV estimation:

$$PV_{sp} = \sum_{c \in \mathbb{C}} \alpha_c \sum_{(u,v)} I_c(u,v) w(u,v), \quad (5)$$

with  $I_c$  the intensity of color channel  $c \in \mathbb{C} = \{R, G, B\}$  of pixel  $(u, v)$ . In the following we will refer to the model in Eq. 5 as the **Linear** model for PV estimation (the parameters,  $\alpha_c$ , of this model are obtained using linear regression).

3) *Saturation*: Let us call  $\mathbb{S}_c = \{(u, v) | I(u, v) = I_{max}\}$  the set of saturated pixels,  $\tilde{I}_c(u, v)$  the pixel intensity if there were no saturation, and  $I_{max}$  the saturation value. Then we estimate PV generation taking into account saturation using:

$$PV_s = PV_{sp} + \sum_{c \in \mathbb{C}} \alpha'_c \sum_{(u,v) \in \mathbb{S}_c} (\tilde{I}_c(u, v) - I_{max}) w(u, v). \quad (6)$$

Given that we do not know the value  $\tilde{I}_c(u, v)$  due to pixel saturation, we estimate the PV generation using a **Non-Linear** regression that uses all known terms in Eq. (6):

$$\hat{y} = F \left( \sum_{(u,v) \in \mathbb{N}_c} I_c(u, v) w(u, v), \sum_{(u,v) \in \mathbb{S}_c} w(u, v), |\mathbb{S}_c| \right). \quad (7)$$

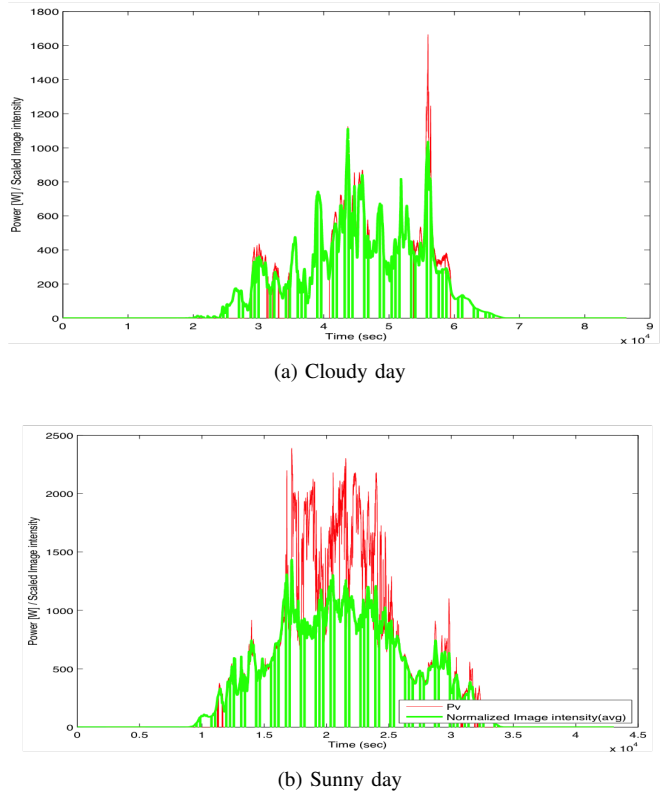


Fig. 6. PV generation (red) vs average image intensity (green). In the case of a cloudy day the average image intensity is a good predictor of the PV generation, but in a sunny day (right) this does not hold due to the camera sensor saturation.

TABLE II  
PV ESTIMATION EVALUATION. SEE FIG. 7 FOR PLOTS OF THE RESULTS.

Data (Figure)	RAE $E_1$ [%]		RMSE $E_2$ [%]	
	Linear	Non-Linear	Linear	Non-Linear
Cloudy (7a)	11.85	7.78	13.71	9.68
Partly cloudy (7b)	20.11	14.14	30.97	22.58
Partly cloudy (7c)	24.67	14.34	28.64	20.11
Sunny (7d)	25.63	13.36	26.59	14.37
Complete test set	25.52	18.27	32.9	24.16

Namely the weighted sum of non-saturated pixels, the sum of the weights of saturated pixels, and the number of saturated pixels  $|\mathbb{S}_c|$ ), for all colors channels (with  $\mathbb{N}_c$  the set of non-saturated pixels for channel  $c$ ) are used. The rationale is that the number of saturated pixels per color channels can provide information regarding the saturated regions.

4) *Experiments in PV estimation*: To test the PV estimation we consider the two cases described above: **Linear** and **Non-Linear** regression, i.e. Eq. 5 and Eq. 7 respectively. This is done using Matlab function ‘fitlm’.

We evaluate the accuracy using two measures: the relative absolute error rate (RAE):

$$E_1 = 100 \frac{1}{T} \sum_t |y(t) - \hat{y}(t)| / y(t), \quad (8)$$

and the root mean squared error rate (RMSE):

$$E_2 = 100 \sqrt{\frac{1}{T} \sum_t (y(t) - \hat{y}(t))^2 / \bar{y}}, \quad (9)$$

with  $y(t)$  the ground truth,  $\hat{y}(t)$  the predicted value, and  $T$  the number of samples.

The regression models are estimated using 56 days worth of data, and evaluated using data from 28 days (different from the ones used for building the regression model). Figure 7 and Table II show results under some typical weather conditions. From these results we can see that

- The relative absolute error rate ( $E_1$ ) for all test videos is 25.52%, and 18.27% for the **Linear** case (Eq. 5) and the **Non-Linear** case (Eq. 7) respectively.
- The root mean squared error rate ( $E_2$ ) for all test videos is 32.9%, and 24.16% for the **Linear** estimation (Eq. 5) and **Non-Linear** estimation (Eq. 7) respectively.
- For a cloudy day case (Fig. 7a), we observe that  $E_1$  is 11.85%, and 7.78% for the linear estimation (Eq. 5) and the non-linear estimation (Eq. 7) respectively. The good performance is due to the low pixel saturation.
- For a sunny day case (Fig. 7d), i.e. pixel saturation, we observe that  $E_1$  is 25.63%, and 13.36% for the linear estimation (Eq. 5) and the non-linear estimation (Eq. 7) respectively. In this case the error, compared to the cloudy day, is almost doubled.

In summary, the method is accurate when the image is not saturated, and explicitly using information of the saturation further improves when saturation occurs.

#### IV. CONCLUSIONS

We have presented a system for sub-minute (1-60 sec.) PV prediction based on the analysis of sky images and cloud movement. This system is location-independent, and it does not require historical data nor dynamical models.

Target applications of this sub-minute prediction system include: *i*) enhancing energy management systems (at homes, factories, etc.), *ii*) improving the management of distribution & transmission networks, and *iii*) reducing the need of backup generation capacity. Also, sky and cloud analysis can be useful for weather prediction and atmospheric studies.

Future research directions include: layered cloud movement analysis, cloud transparency estimation, prediction of sun occlusion, and formulating a model of the sky image intensity that takes into account Mie scattering and Rayleigh scattering.

#### ACKNOWLEDGMENTS

This work was partially supported by the JSPS Kakenhi grant 17H01922, the i-Energy joint research chair, Kyoto University, by the Research Unit for Smart Energy Management, Kyoto University, and by Panasonic, Japan.

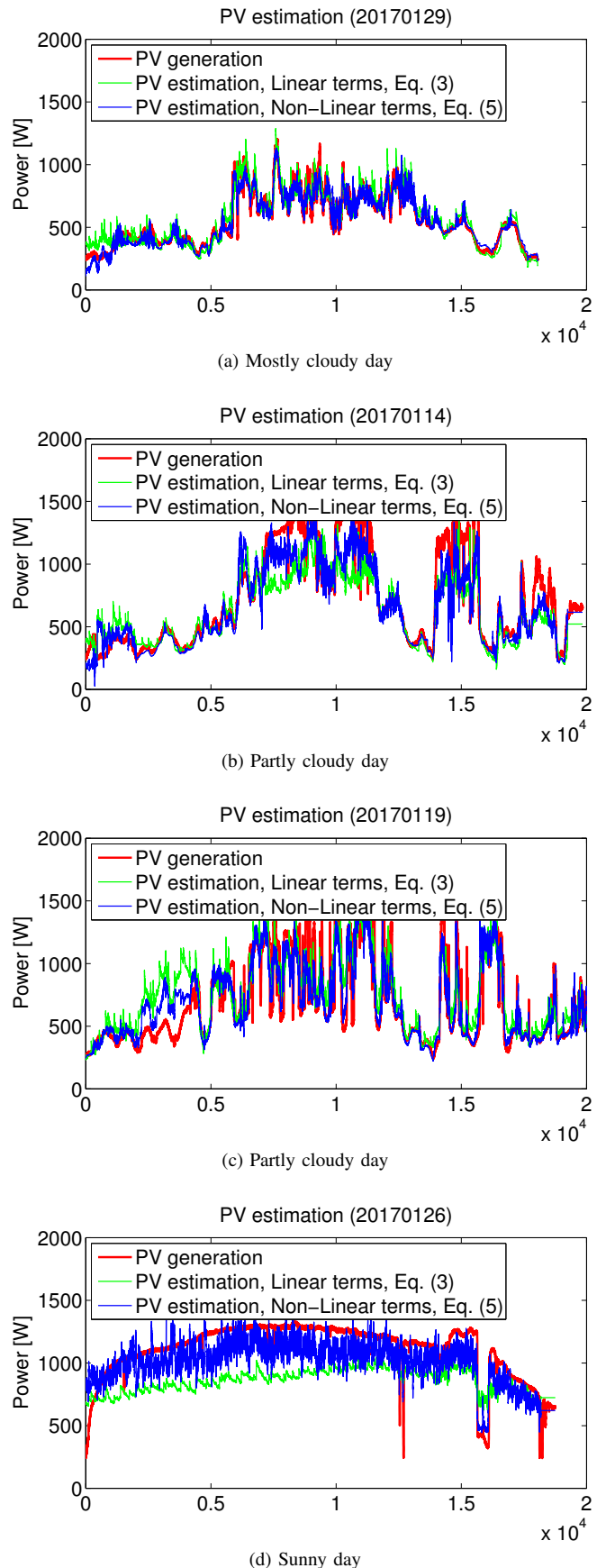


Fig. 7. PV estimation. Linear regression is used for PV estimation. The usage of information regarding pixel saturation (blue) improves the results, in particular during sunny periods.

## REFERENCES

- [1] T. Kato, K. Tamura, and T. Matsuyama, "Adaptive storage battery management based on the energy on demand protocol," in *2012 IEEE Int. Conf. on Smart Grid Communications (SmartGridComm)*, 2012.
- [2] R. Verschae, T. Kato, and T. Matsuyama, "Energy management in prosumer communities: A coordinated approach," *Energies*, vol. 9, no. 7, p. 562, 20 Jul. 2016.
- [3] T. Matsuyama, "i-energy: Smart demand-side energy management," in *Smart Grid Applications and Developments*, ser. Green Energy and Technology, D. Mah, P. Hills, V. O. Li, and R. Balme, Eds. Springer London, 2014, pp. 141–163.
- [4] K. Ogimoto, I. Kaizuka, Y. Ueda, and T. Oozeki, "A good fit: Japan's solar power program and prospects for the new power system," *Power and Energy Magazine, IEEE*, vol. 11, no. 2, pp. 65–74, March 2013.
- [5] V. Kostylev and A. Pavlovski, "Solar power forecasting performance—towards industry standards," in *1st International Workshop on the Integration of Solar Power into Power Systems*, Denmark, 2011.
- [6] J. Kleissl, *Solar energy forecasting and resource assessment*. Academic Press, 2013.
- [7] S. Pelland, G. Galanis, and G. Kallos, "Solar and photovoltaic forecasting through post-processing of the global environmental multiscale numerical weather prediction model," *Progress in Photovoltaics: Research and Applications*, vol. 21, no. 3, pp. 284–296, 2013.
- [8] R. Perez, P. Ineichen, K. Moore, M. Kmiecik, C. Chain, R. George, and F. Vignola, "A new operational model for satellite-derived irradiances: description and validation," *Solar Energy*, vol. 73, no. 5, pp. 307–317, Nov. 2002.
- [9] C. Yang, A. A. Thatte, and L. Xie, "Multitime-Scale Data-Driven Spatio-Temporal forecast of photovoltaic generation," *IEEE Transactions on Sustainable Energy*, vol. 6, no. 1, pp. 104–112, Jan. 2015.
- [10] T. T. Teo, T. Logenthiran, and W. L. Woo, "Forecasting of photovoltaic power using extreme learning machine," in *2015 IEEE Innovative Smart Grid Technologies - Asia (ISGT ASIA)*, Nov. 2015, pp. 1–6.
- [11] B. Urquhart, B. Kurtz, E. Dahlin, M. Ghonima, J. E. Shields, and J. Kleissl, "Development of a sky imaging system for short-term solar power forecasting," *Atmospheric Measurement Techniques*, vol. 8, no. 2, pp. 875–890, 20 Feb. 2015.
- [12] P. E. Debevec and J. Malik, "Recovering high dynamic range radiance maps from photographs," *ACM SIGGRAPH 2008 classes*, 2008.
- [13] D. Scaramuzza and R. Siegwart, "A Practical Toolbox for Calibrating Omnidirectional Cameras," in *Vision Systems: Applications*, G. Obinata and D. Ashish, Eds. I-Tech, 2007.
- [14] B. K. Horn and B. G. Schunck, "Determining optical flow," *Artificial intelligence*, vol. 17, no. 1-3, pp. 185–203, 1981.